INTERNATIONAL JOURNAL FOR NUMERICAL METHODS IN FLUIDS, VOL. 11, 1113–1126 (1990)

# NUMERICAL STUDIES OF FLUID FLOW THROUGH TUBES WITH DOUBLE CONSTRICTIONS

T. S. LEE

*Mechanical and Production Engineering Departments, Faculty of Engineering, National University of Singapore, Singapore 0511*

## SUMMARY

The flow fields in the neighbourhood of double constrictions in a circular cylindrical tube were studied numerically. The effects on the streamline, velocity and vorticity distributions as the flow passes through the constrictions in the tube were studied in the Reynolds number range 5–200. Double constrictions with dimensionless spacing ratios of 1, 2, 3 and $\infty$ were studied for a 50% constriction.

It is noted that when the Reynolds number is below 10, no recirculation region is formed in the above constricted flow. For Reynolds numbers greater than 10, a recirculation region forms downstream of each of the constrictions. For constriction spacing ratios of 1, 2, and 3, when the Reynolds number is high, a recirculation region spreads between the valley of the constrictions. The recirculation region formed between the two constrictions has a diminishing effect on the generation of wall vorticity near the second constriction area. In general, the peak value of wall vorticity is found slightly upstream of each of the constrictions. When the Reynolds number is increased, the peak wall vorticity value increases and its location is moved upstream. Maximum wall vorticity generated by the first constriction is found to be always greater than the maximum wall vorticity generated by the second constriction. The extent of this spreading of the recirculation region from the first constriction and its effects on the second constriction depend on the constriction spacing ratio and the flow Reynolds number.

KEY WORDS Constrictions Recirculation Vorticity Streamline

## INTRODUCTION

The flow field in the neighbourhood of constrictions in tubes has been of great interest to fluid dynamicists because of its many engineering applications. This type of configuration is used in heat exchangers in order to enhance heat transfer performance. A wavy configuration of tubes has also been of great interest to biofluid dynamicists because of its relationship to localized stenoses, blood and urinary flow, and for the optimal design of artificial organs. Similar viscous fluid flow past wavy boundaries has also been of great interest to researchers because of its importance in phenomena such as the generation of wind waves on water, the stability of a liquid film in contact with a gas stream, the transpiration cooling of re-entry vehicles and rocket boosters, film vaporization in combustion, fluid flow in pipes with fittings, etc.

An earlier numerical work on this type of problem was done by Lee and Fung[1] to study the flow in locally constricted tubes in the Reynolds number range 0–25. A bell-shaped constriction specified by a Gaussian normal distribution curve was used. Similar numerical studies were carried out by Oberkampf and Goh.[2] An outflow-type boundary condition was used by Lee and Fung, whilst Oberkampf and Goh used an infinity condition. Constrictions with other type of profiles such as a sinusoidal function were used by Desphande *et al.*[3] to model the steady laminar

0271–2091/90/161113–14$07.00

*Received October 1989*
*Revised January 1990*

flow through vascular stenoses. A survey of the numerical methods used for constricted physiological flows was presented by Mueller.[4] The separating flow through a severely constricted symmetric tube was studied analytically by Smith.[5] The main separation was shown to take place on the upstream constriction surface. In more recent work, Wille[6] studied the pressure and flow fields in arterial stenoses simulated by mathematical models. Sobey[7] studied numerically the flow through furrowed channels and investigated the Reynolds number effects on the separated flow. Stephanoff *et al.*[8] compared the numerical results of Sobey with experimental observations through flow visualization techniques. Velocity measurements in the neighbourhood of axisymmetric constrictions in rigid tubes were investigated by Ahmed and Giddens[9] using laser Doppler anemometry and hydrogen flow visualization techniques. Experimental flow visualization of streamlines in steady flow through constrictions was also obtained by Siouffi *et al.*[10] in a study on the effects of unsteadiness on the flow through stenoses. Prata and Sparrow[11] obtained numerical solutions for a periodic, fully developed regime in an annulus of varying cross-section of double pipe in a heat exchanger. On the basis of the computed heat transfer coefficients and pressure drops, the periodic annulus appears to be an attractive enhancement of the configuration relative to the annulus of axially unchanging cross-section. Other related recent studies of constricted flow include a study of laminar steady flow in sinusoidal channels by Tsangaris and Leiter[12] using a perturbation technique. O'Brien and Ehrlich[13] studied numerically the pulsatile flow through a constricted artery using conformal mapping. Experimental measurements and prediction of flow through a replica segment of a mildly atherosclerotic coronary artery were done by Back *et al.*[14]

In the present work the flow behaviour in a double constricted symmetrical tube was studied numerically using a finite difference model. The double bell-shaped constricted tube was transformed into a rectangular solution domain using a generalized mapping function. The dynamics of the flow describing separation, reattachment and the formation of recirculation eddy were revealed by the streamline, velocity and vorticity fields. Numerical results were obtained for Reynolds numbers in the range 5–200 with a 50% constriction. Constrictions with dimensionless constriction spacing ratios of 1, 2, 3 and $\infty$ were studied. The findings of the present study were also compared with available experimental and numerical work of other investigators.

## PROBLEM FORMULATION

The geometrical configuration of the tube with double constrictions and its co-ordinate system is shown in Figure 1(a). The unsteady governing equations are used to solve for the steady state flow fields considered in this study. Constant fluid properties are assumed and the flow is considered axisymmetric and laminar. The governing equations are:

*momentum equations*

$$\frac{\partial v_r}{\partial t} + v_r \frac{\partial v_r}{\partial r} + v_z \frac{\partial v_r}{\partial z} = -\frac{1}{\rho}\frac{\partial p}{\partial r} + \nu\left(\frac{\partial^2 v_r}{\partial r^2} + \frac{\partial^2 v_r}{\partial z^2} + \frac{1}{r}\frac{\partial v_r}{\partial r} - \frac{v_r}{r^2}\right), \tag{1}$$

$$\frac{\partial v_z}{\partial t} + v_r \frac{\partial v_z}{\partial r} + v_z \frac{\partial v_z}{\partial z} = -\frac{1}{\rho}\frac{\partial p}{\partial z} + \nu\left(\frac{\partial^2 v_z}{\partial r^2} + \frac{\partial^2 v_z}{\partial z^2} + \frac{1}{r}\frac{\partial v_z}{\partial r}\right), \tag{2}$$

*continuity equation*

$$\frac{\partial v_r}{\partial r} + \frac{v_r}{r} + \frac{\partial v_z}{\partial z} = 0. \tag{3}$$

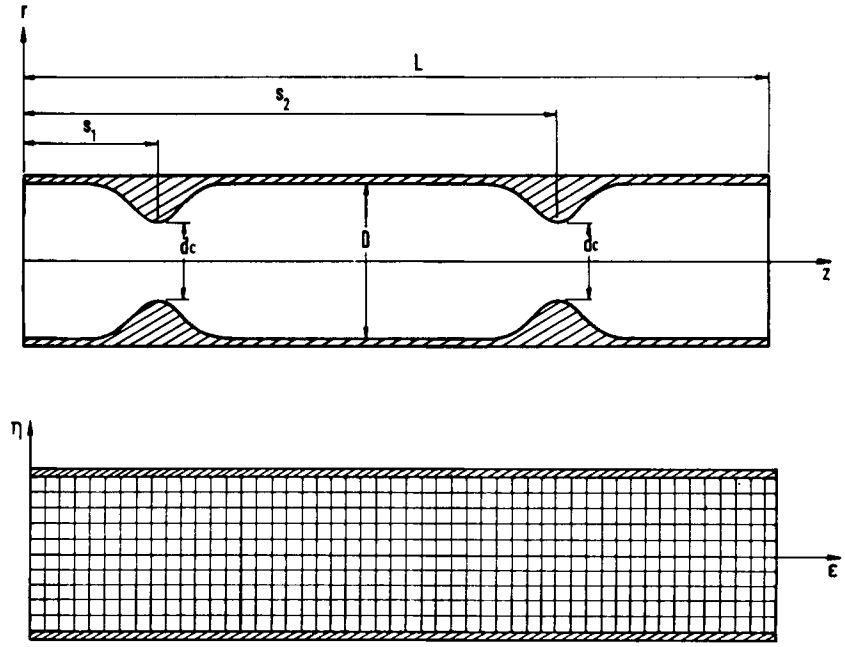


Figure 1. Model of the double constriction tube and its co-ordinate systems: (a) The original physical space; (b) The Transformed solution domain

The vorticity $\zeta$ is defined as

$$\zeta = \frac{\partial v_r}{\partial z} - \frac{\partial v_z}{\partial r}. \tag{4}$$

By eliminating the pressure terms in equations (1) and (2), and with the use of equation (3) together with the definition of vorticity given by equation (4), the vorticity transport equation is obtained as

$$\frac{\partial \zeta}{\partial t} + \frac{\partial (v_r \zeta)}{\partial r} + \frac{\partial (v_z \zeta)}{\partial z} = \nu \left( \frac{\partial^2 \zeta}{\partial r^2} + \frac{\partial^2 \zeta}{\partial z^2} + \frac{1}{r}\frac{\partial \zeta}{\partial r} - \frac{\zeta}{r^2} \right). \tag{5}$$

The incompressible streamfunction $\psi$ is defined by

$$v_r = \frac{1}{r}\frac{\partial \psi}{\partial z}, \qquad v_z = -\frac{1}{r}\frac{\partial \psi}{\partial r}, \tag{6}$$

where $v_r$ and $v_z$ are the velocity components in the $r$- and $z$-directions respectively.

Hence equation (4) can be expressed as

$$\zeta = \frac{1}{r}\left( \frac{\partial^2 \psi}{\partial r^2} + \frac{\partial^2 \psi}{\partial z^2} - \frac{1}{r}\frac{\partial \psi}{\partial r} \right). \tag{7}$$

From the geometry of the constriction, the tube radius $a_0$ is identified as a characteristic length. The inlet velocity $v_\infty$ on the axis of the tube far away from the constriction is taken as the

characteristic velocity. The following dimensionless variables are defined:

$$r^* = r/a_0, \qquad z^* = z/a_0, \qquad v_r^* = v_r/v_\infty, \qquad v_z^* = v_z/v_\infty,$$
$$\psi^* = \psi/(v_\infty a_0^2), \qquad \zeta^* = \zeta/(v_\infty/a_0), \qquad t^* = t/(a_0/v_\infty). \tag{8}$$

The dimensionless vorticity transport equation can then be expressed as

$$\frac{\partial \zeta^*}{\partial t^*} + \frac{\partial (v_r^* \zeta^*)}{\partial r^*} + \frac{\partial (v_z^* \zeta^*)}{\partial z^*} = \frac{1}{Re}\left( \frac{\partial^2 \zeta^*}{\partial r^{*2}} + \frac{\partial^2 \zeta^*}{\partial z^{*2}} + \frac{1}{r^*}\frac{\partial \zeta^*}{\partial r^*} - \frac{\zeta^*}{r^{*2}} \right), \tag{9}$$

where the Reynolds number $Re = v_\infty a_0/\nu$.

The dimensionless vorticity–streamfunction equation becomes

$$\zeta^* = \frac{1}{r^*}\left( \frac{\partial^2 \psi^*}{\partial r^{*2}} + \frac{\partial^2 \psi^*}{\partial z^{*2}} - \frac{1}{r^*}\frac{\partial \psi^*}{\partial r^*} \right) \tag{10}$$

and the dimensionless velocities are

$$v_r^* = \frac{1}{r^*}\frac{\partial \psi^*}{\partial z^*}, \qquad v_z^* = -\frac{1}{r^*}\frac{\partial \psi^*}{\partial r^*}. \tag{11}$$

(In subsequent expressions the asterisk is dropped for simplicity.)

In dimensionless form the geometry of the constrictions may be described by the following bell-shaped Gaussian distribution profile:

$$f(z) = 1 - c_1 \exp[-c_2(z - s)^2], \tag{12}$$

where $c_1$ is the constriction ratio ($= (D - d_c)/D$), $c_2$ is a shape constant and $s$ is the dimensionless distance of the constriction from the inlet plane.

Referring to Figure 1(a), for the double constrictions considered here, $c_1 = 0{\cdot}5$, $c_2 = 0{\cdot}4$, $s = s_1$ for $z_1 < z < z_2$, $s = s_2$ for $z_3 < z < z_4$ and $c_1 = 0$ elsewhere; $z_1$ and $z_2$ are the upper and lower limits of the first constriction; $z_3$ and $z_4$ are the upper and lower limits of the second constriction; $s_1$ and $s_2$ are the distances of the first and second constrictions from the inlet plane respectively. The spacing between the two constrictions is given by $S = s_1 - s_2$, and $s_1 = 2{\cdot}0$ in this study. When the dimensionless spacing ratio $S/D = \infty$, this is equivalent to a single constriction tube with $c_1 = 0{\cdot}5$, $c_2 = 0{\cdot}4$, $s = s_1$ for $z_1 < z < z_2$ and $c_1 = 0$ elsewhere.

For the present studies the incoming flow is assumed to be Poiseuillean and the outflow is assumed to be unrestricted. A non-slip boundary condition is assumed for the tube wall. The flow is assumed to be symmetrical about its axis, with $v_r = 0$ axis, i.e.

| | | |
|---|---|---|
| at the inlet | $v_r = 0,$ | $v_z = 1 - r^2,$ |
| at the outlet | $\partial v_r/\partial z = \partial v_z/\partial z = 0,$ | |
| along the tube axis | $v_r = 0,$ | $\partial v_z/\partial r = 0,$ |
| along the tube wall | $v_r = v_z = 0.$ | |

(13)

The boundary streamfunction values follow closely from those of the velocity boundary conditions described above. $\psi = 0$ is arbitrarily chosen along the axis of the tube. The inlet and tube wall streamfunctions are then obtained from the assumed inlet velocity distribution. The outlet streamfunction is obtained from the above assumption of unrestricted flow. From the definition of vorticity given in equation (9), the vorticity boundary conditions follow those of the streamfunction and the velocity boundary conditions.

## NUMERCIAL SOLUTION

The cylindrical $(r, z)$ co-ordinate system shown in Figure 1(a) is not suitable for accurate evaluation of the numerical solution near the irregular boundary. One of the most efficient methods of dealing with this problem is to use a co-ordinate transformation as shown in Figure 1(b). The tube with the bell-shaped constrictions is mapped into a rectangular solution domain and the flow fields are solved with a finite difference method. The new co-ordinate system is defined as follows:

$$\varepsilon = F_1(z) = z, \qquad \eta = F_2(r, z) = r/f(z). \tag{14}$$

Expressing the partial derivatives in the new co-ordinates, the governing equations become

$$\frac{\partial \zeta}{\partial t} + \frac{\partial (v_r \zeta)}{\partial \eta}\frac{\mathrm{d}\eta}{\mathrm{d}r} + \frac{\partial (v_z \zeta)}{\partial \varepsilon}\frac{\mathrm{d}\varepsilon}{\mathrm{d}z} + \frac{\partial (v_z \zeta)}{\partial \eta}\frac{\mathrm{d}\eta}{\mathrm{d}z} = \frac{1}{Re}\left\{\frac{\partial^2 \zeta}{\partial \eta^2}\left[\left(\frac{\mathrm{d}\eta}{\mathrm{d}r}\right)^2 + \left(\frac{\mathrm{d}\eta}{\mathrm{d}z}\right)^2\right] + \frac{\partial^2 \zeta}{\partial \varepsilon^2}\left(\frac{\mathrm{d}\varepsilon}{\mathrm{d}z}\right)^2 + \frac{\partial^2 \zeta}{\partial \eta \partial \varepsilon}\left(2\frac{\mathrm{d}\eta}{\mathrm{d}z}\frac{\mathrm{d}\varepsilon}{\mathrm{d}z}\right) + \frac{\partial \zeta}{\partial \eta}\left(\frac{\partial^2 \eta}{\partial z^2} + \frac{1}{r}\frac{\mathrm{d}\eta}{\mathrm{d}r}\right) + \frac{\partial \zeta}{\partial \varepsilon}\left(\frac{\mathrm{d}^2 \varepsilon}{\mathrm{d}z^2}\right) - \frac{\zeta}{r^2}\right\}, \tag{15}$$

$$\zeta = \frac{1}{r}\left\{\frac{\partial^2 \psi}{\partial \eta^2}\left[\left(\frac{\mathrm{d}\eta}{\mathrm{d}r}\right)^2 + \left(\frac{\mathrm{d}\eta}{\mathrm{d}z}\right)^2\right] + \frac{\partial^2 \psi}{\partial \varepsilon^2}\left(\frac{\mathrm{d}\varepsilon}{\mathrm{d}z}\right)^2 + \frac{\partial^2 \psi}{\partial \eta \partial \varepsilon}\left(2\frac{\mathrm{d}\eta}{\mathrm{d}z}\frac{\mathrm{d}\varepsilon}{\mathrm{d}z}\right) + \frac{\partial \psi}{\partial \varepsilon}\left(\frac{\mathrm{d}^2 \varepsilon}{\mathrm{d}z^2}\right) + \frac{\partial \psi}{\partial \eta}\left(\frac{\partial^2 \eta}{\partial z^2} - \frac{1}{r}\frac{\mathrm{d}\eta}{\mathrm{d}r}\right)\right\}. \tag{16}$$

The velocities are

$$v_r = \frac{1}{r}\left(\frac{\partial \psi}{\partial \eta}\frac{\mathrm{d}\eta}{\mathrm{d}z} + \frac{\partial \psi}{\partial \varepsilon}\frac{\mathrm{d}\varepsilon}{\mathrm{d}z}\right), \qquad v_z = -\frac{1}{r}\left(\frac{\partial \psi}{\partial \eta}\frac{\mathrm{d}\eta}{\mathrm{d}r} + \frac{\partial \psi}{\partial \varepsilon}\frac{\mathrm{d}\varepsilon}{\mathrm{d}r}\right), \tag{17}$$

where $z = \varepsilon$, $r = \eta f(\varepsilon)$ and $\mathrm{d}\varepsilon/\mathrm{d}r = 0$, $\mathrm{d}\varepsilon/\mathrm{d}r = 1$.

Similarly, the boundary conditions for the streamfunctions, velocities and vorticity are also expressed in the $\varepsilon$–$\eta$ co-ordinate system.

The rectangular domain in the $\varepsilon$–$\eta$ co-ordinate system in Figure 1(b) is overlaid with a regular finite difference mesh. At the node points the finite difference solutions to equation (15) with their boundary conditions are obtained through an alternating direction implicit (ADI) procedure proposed by Samarskii and Andreev.[15] The successive overrelaxation (SOR) method with a relaxation parameter $\omega = 1{\cdot}1$ is used to solve the vorticity–streamfunction equation (16). All spatial derivatives are approximated by second-order-accurate central differences. The convective terms in equation (15) are approximated by the second-order upwind differencing method. Three-point backward and forward difference formulae are used for the derivatives at the boundaries. The vorticity boundary values are obtained by considering the Taylor series expansion of $\psi$ into the solution region and taking into consideration the $\psi$ and the velocity at the boundary. The mesh size used for the solutions illustrated here is $21 \times 151$. The steady state solution of equations (15) and (16) is said to have converged when a difference of 0·01% of a referenced $\psi$ and $\eta$ is detected. This has prove satisfactory. The streamfunction contours, the velocity fields and the vorticity contours are noted to be steady after the above criteria are satisfied.

## RESULTS AND DISCUSSION

Characteristics of the recirculating flow region and flow through the constrictions were investigated for constriction spacing ratios of 1, 2, 3 and $\infty$. The streamlines and vorticity distributions for this investigation are shown in Figure 2. At a low Reynolds number of 5 (Figure 2(a)) the streamlines and vorticity contours for constriction spacing ratios of 1, 2, 3 and $\infty$ are similar. The flow around each constriction of the double constriction tube behaves in a manner similar to that in an independent single constriction tube, i.e. without any interference of the flows with each other. Hence the vorticity contours are also similar near each of the constrictions. No recirculation region appears in the constricted tube at a Reynolds number of 5. As the Reynolds number approaches 10 (Figure 2(b)), a recirculation eddy appears downstream of each constriction. At a Reynolds number greater than 50 (Figure 2(c)) the vorticity fields are substantially altered and the closed contours of the vorticity distribution are seen to be advected downstream from each constriction. The recirculatory eddy from the upstream constriction is also spread downstream and this affects the flow passing through the downstream constriction. A recirculation zone now exists which fills part of the valley region between the two constrictions. Once the recirculation flow field between the constrictions is established, there is a separation streamline that divides the

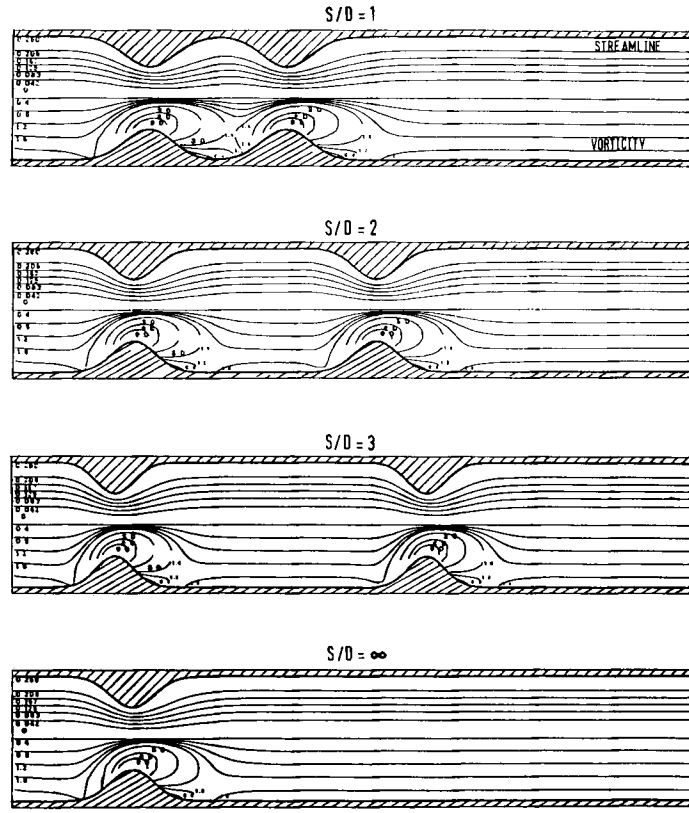


(a) REYNOLDS NUMBER = 5

Figure 2. (a)

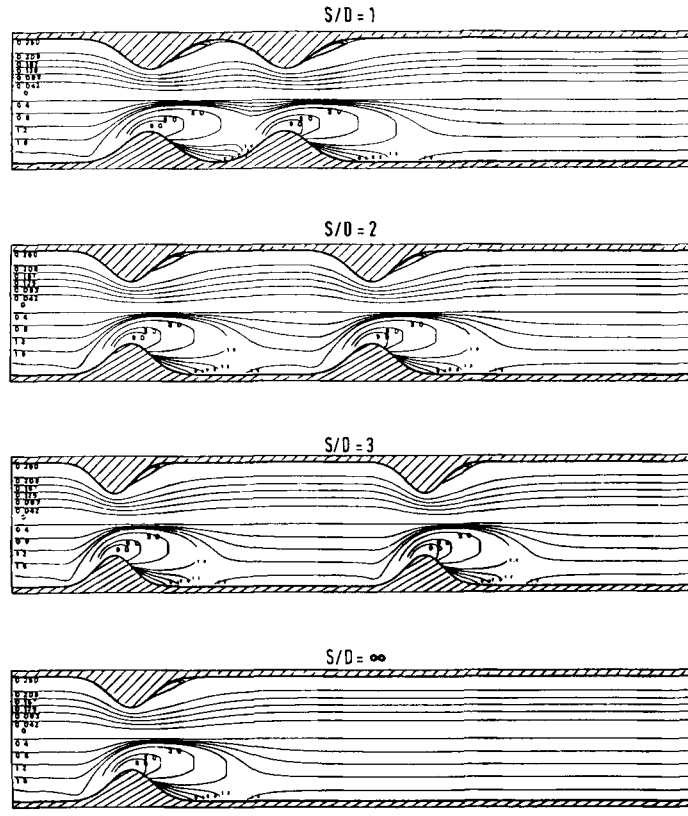


(b) REYNOLDS NUMBER = 10

Figure 2. (b)

flow into two parts: the recirculating flow field between the two constrictions and the main flow field near the centre of the tube with relatively straight and parallel streamlines.

The separation and reattachment points of the recirculation eddies formed downstream of each of the constrictions for different constriction spacing ratios are shown in Figure 3. It can be seen that when the Reynolds number is increased, the separation point on the surface of the constriction where the recirculation eddy begins to form moves slightly upstream of the throat. The reattachment point where the recirculation eddy terminates on the surface of he constricted tube spreads downstream of the throat. When a steady recirculation region is established between the two constrictions, there is then little change to the separation and reattachment points for the flow in the valley region. However, the reattachment point of the downstream constriction spreads further as the Reynolds number is increased and eventually approaches that of a single constriction corresponding to $S/D = \infty$.

The variations of the centreline velocities due to the influence of the constriction spacing ratios and Reynolds numbers are shown in Figure 4. For a Reynolds number greater than 5 it is noted that the maximum centreline velocity does not occur at the throat. At this point the fluid is still experiencing an acceleration, so that the maximum centreline velocity in the field occurs slightly downstream of each of the constrictions. At higher Reynolds number ($Re \geqslant 25$), where a zone of

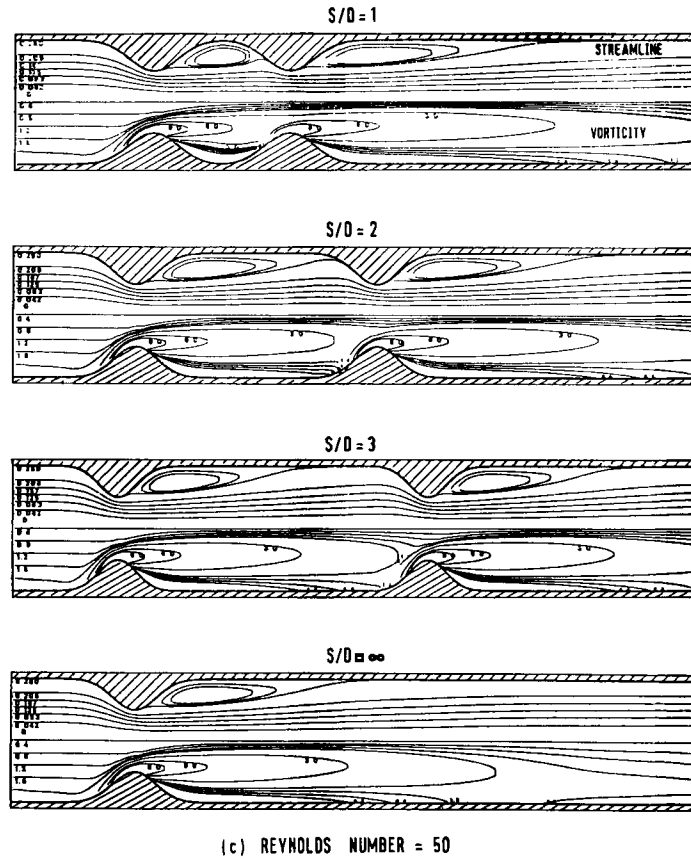


Figure 2. Streamline profiles for different constriction spacings: (a) $Re = 5$; (b) $Re = 10$; (c) $Re = 50$

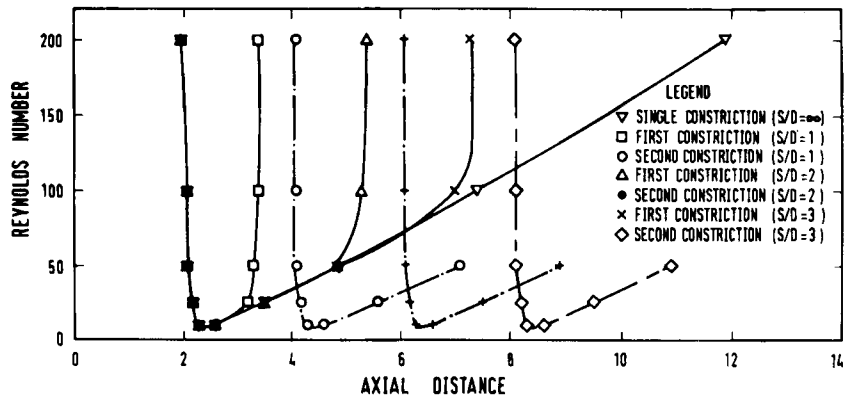


Figure 3. Separation and reattachment of flow for different constriction spacings

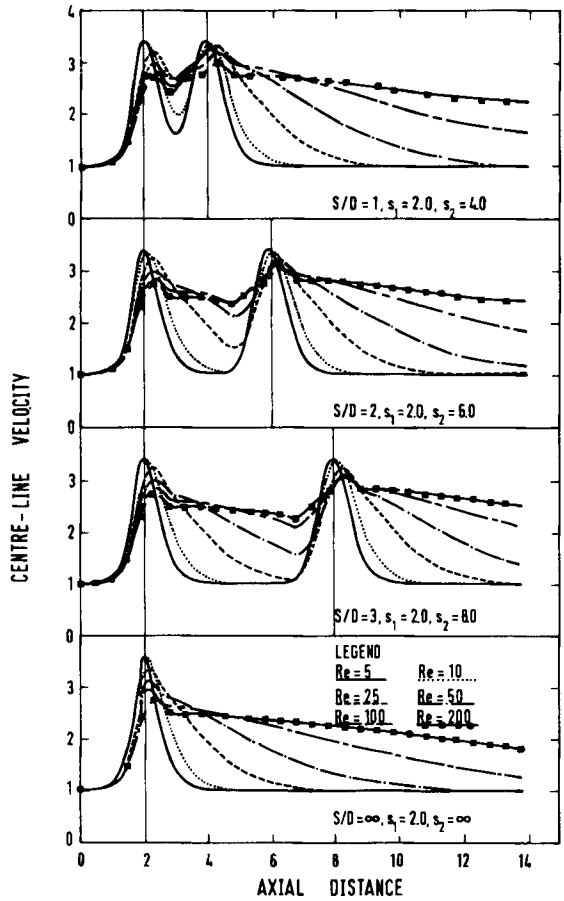


Figure 4. Variation of centreline velocity for different constriction spacings

recirculation is established between the constrictions with $S/D = 1, 2$ and 3, the centreline velocity does not have the opportunity to recover fully before passing through the second constriction. Note that the maximum centreline velocity shifts downstream as the Reynolds number increases; the maximum value near the second constriction is also slightly higher than the maximum value at the first constriction.

Characteristics of the flow through constrictions can also be described by the velocity vector in the tube. The velocity vectors in Figure 5 show that as the fluid flows into the converging portion of the constriction, the velocity increases in magnitude and the vectors point towards the axis of the tube. The formation of the recirculation region in the flow is indicated by the negative velocity vectors in a reversed flow. The wall vorticity values, which are related to the velocity distribution, are also of considerable interest to researchers since they are related to the wall shear stress. As shown in Figure 5, the magnitude of the wall vorticity value increases rapidly when the flow approaches the constriction, and reaches a peak value near the maximum constricted area for a Reynolds number less than or equal to 10. At higher Reynolds numbers the peak wall vorticity value is found slightly upstream of the maximum constricted area. At a location downstream of this peak value the wall vorticity decreases rapidly and will reverse to negative values when

separation begins at the wall of the tube. It is observed that the peak wall vorticity value increases with increasing Reynolds number. For the present investigation with $S/D = \infty$ (Figure 5(c)) the peak wall vorticity value is 24·02 at a Reynolds number of 5; this increases to 57·31 when the Reynolds number is increased to 200. The location of the peak wall vorticity value tends to shift upstream as the Reynolds number is increased. The negative wall vorticity values also give an indication of the extent of the recirculation region in the constricted flow. For Reynolds numbers greater than 10, negative wall vorticity values are found at the tube surface owing to the existence of the recirculation eddy downstream of the constriction. The negative magnitude of the wall vorticity value in the recirculation region increases when the Reynolds number is increased. At a Reynolds number of 200 there is a large region of recirculatory flow in the constricted tube, as shown by the extent of negative wall vorticity distribution along the tube wall. With $S/D = 1, 2$ and 3 the recirculation eddy formed downstream of the first constriction has a diminishing effect

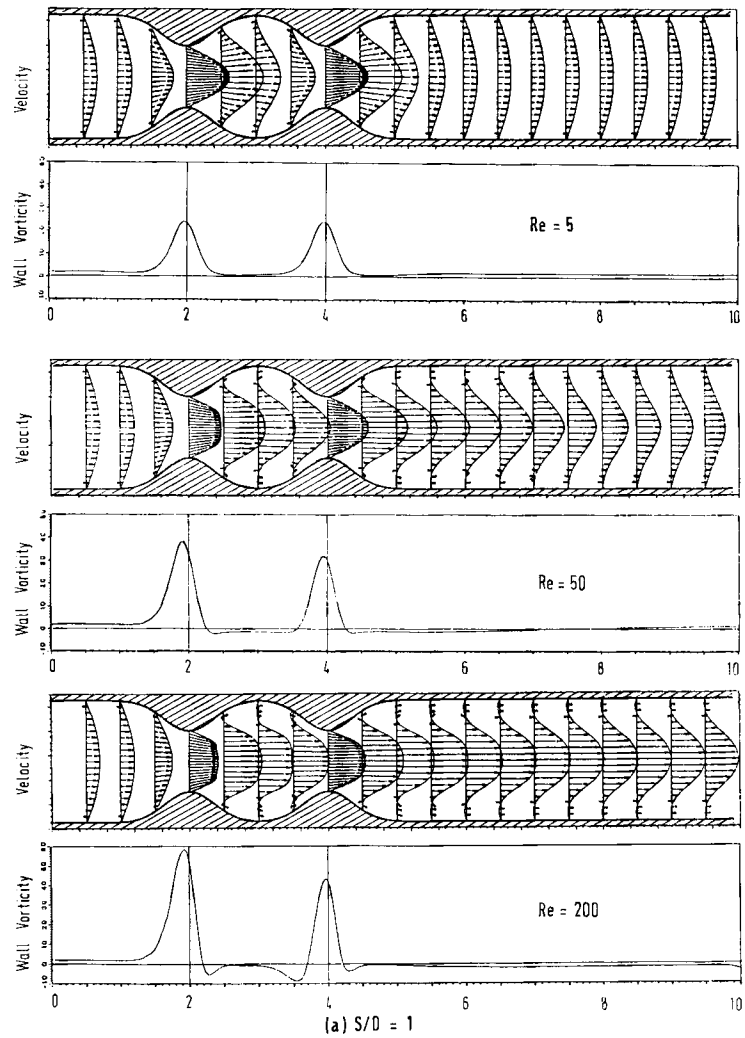


Figure 5. (a)

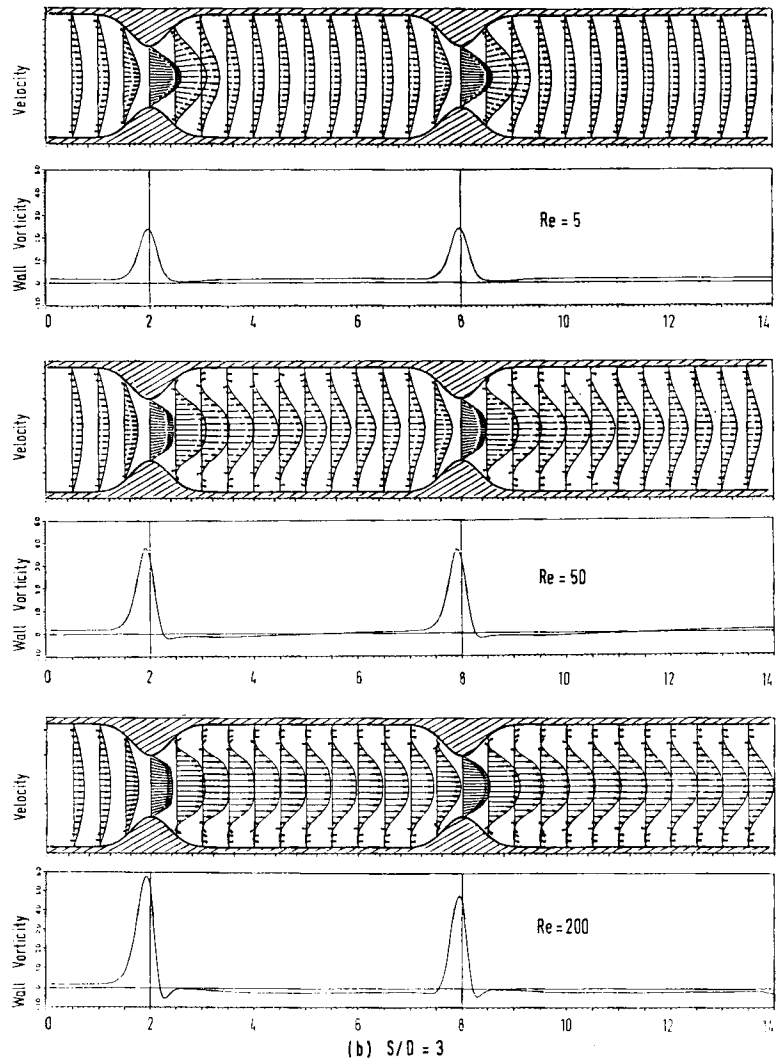


Figure 5. (b)

on the generation of vorticities by the main stream near the second constriction area. The main stream approaching the second constriction wall is straightened by the recirculation region formed in the valley. Hence the maximum wall vorticity generated by the first constriction is always greater than the maximum wall vorticity generated by the second constriction. The maximum wall vorticity values obtained for spacing ratios of 1, 2 and 3 when the flow passes through the second constriction are always lower than those obtained for a constriction spacing ratio of $\infty$.

The present study with $S/D = \infty$ is also equivalent to a study of the single constriction tube. This is similar to a study by Lee and Fung[1] where numerical results were obtained for Reynolds numbers in the range 0–25. The corresponding streamlines, vorticity and velocity distributions for the present investigation are shown in Figures 2 and 5(c) for the Reynolds number range

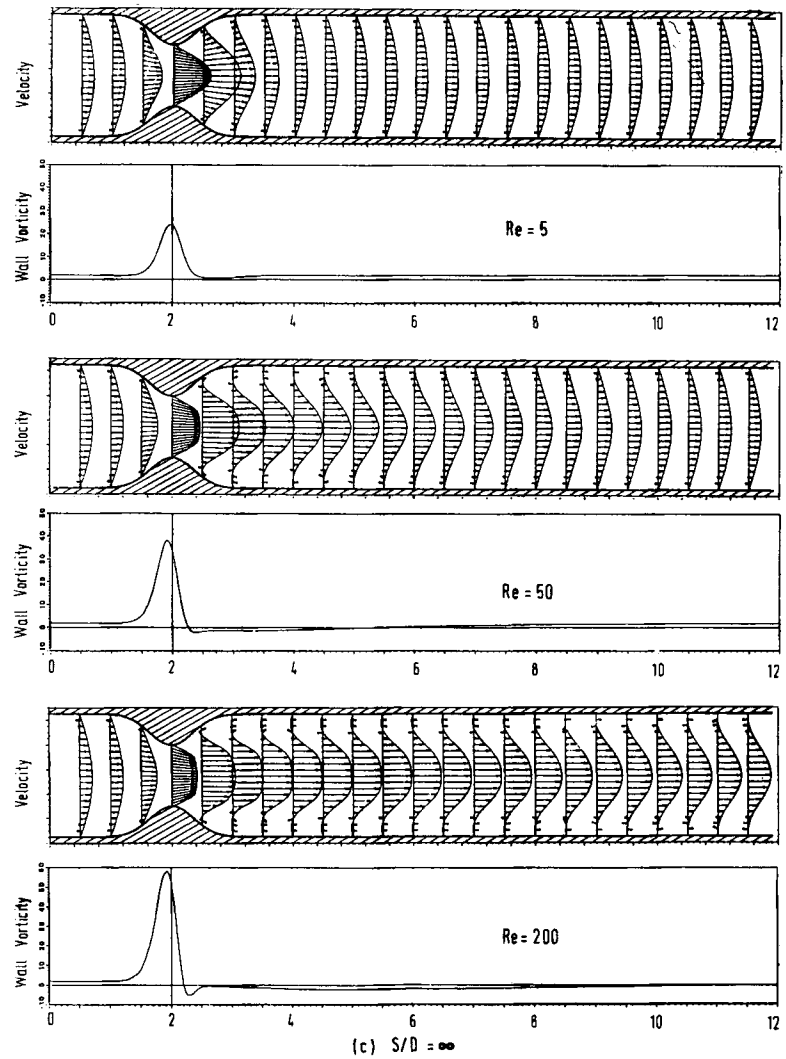


Figure 5. Velocity vectors and wall vorticity distributions for different constriction spacings: (a) $S/D = 1$; (b) $S/D = 3$; (c) $S/D = \infty$

5–200. The streamlines, vorticity and velocity profiles show striking similarities between the two investigations in the Reynolds number range 5–25. At $Re = 9{\cdot}9$ an eddy was observed just downstream of the constriction by Lee and Fung. A similar eddy was also observed in the present study at $Re = 10$. The study of Lee and Fung showed that the location of the maximum wall vorticity shifts slightly upstream of the throat as the Reynolds number is increased. This flow behaviour was also observed in the present study. Lee and Fung obtained maximum wall vorticities of 28·5 and 36·5 at Reynolds numbers of 10 and 25 respectively. The corresponding values obtained in the present investigation were 24·62 and 29·84. The difference is believed to be due to the manner in which the outlet boundary condition was formulated. Lee and Fung assumed the outflow was Poiseuillean, whilst the present study assumed an unrestricted flow at the outlet and allowed the flow profile to develop on its own. An experimental study of a similar

constriction was presented by Bentz and Evans.[16] Velocity profiles were obtained using a laser Doppler velocimeter for steady state results with Reynolds numbers in the range 2–170. A comparison of these experimental results with the results of the present study for Reynolds numbers in the range 5–200 shows similar velocity profiles.

## CONCLUSIONS

Numerical solutions to the flow fields in the neighbourhood of double symmetrical bell-shaped constrictions in a circular cylindrical tube were obtained for a Reynolds number range 5–200 with constriction spacing ratios of 1, 2, 3 and $\infty$. For the present study with a constriction of 50%, a recirculation eddy is found to occur downstream of the constriction when the Reynolds number is increased to 10. When the Reynolds number is further increased, the point of separation of the eddy moves upstream of the constriction and the reattachment point moves downstream. At higher Reynolds numbers a recirculation zone fills the valley region between the two constrictions. A separation streamline then divides the flow into two parts: the recirculation region in the valley, and a relatively straight and parallel flow near the centre of the tube. The maximum centreline velocity shifts downstream as the Reynolds number increases, and the maximum value at the second constriction is also higher than the maximum value at the first constriction. In contrast, the local maximum wall vorticity value always occurs slightly upstream of each of the constrictions, and the maximum wall vorticity value at the second constriction is always less than the maximum wall vorticity value at the first constriction.

### ACKNOWLEDGEMENT

This work was sponsored by the University of Singapore under research grants RP 25/85 and RP 890633.

## APPENDIX: NOMENCLATURE

| | |
|---|---|
| $(r, z)$ | co-ordinate variables in the original cylindrical co-ordinate system |
| $a_0$ | radius of the tube having a constant cross-section |
| $D$ | diameter of the tube having a constant cross-section |
| $d_c$ | opening of the constriction |
| $L$ | length of the tube |
| $s_1, s_2$ | distance of first and second constrictions from inlet plane |
| $S$ | spacing between constrictions, $S = s_2 - s_1$ |
| $u$ | radial velocity component |
| $v$ | axial velocity component |
| $v_\infty$ | axial velocity at infinity |
| $z_1, z_2$ | limits of first constriction |
| $z_3, z_4$ | limits of second constriction |
| $(\eta, \varepsilon)$ | co-ordinate variables in the transformed co-ordinate system |
| $\psi$ | streamfunction |
| $\zeta$ | vorticity |
| $t$ | time |
| $Re$ | Reynolds number |
| $p$ | pressure |
| $\rho$ | density |

| | |
|---|---|
| $\nu$ | kinematic viscosity |
| $\Delta\eta$ | incremental step in radial direction of transformed mesh |
| $\Delta\varepsilon$ | incremental step in axial direction of transformed mesh |
| $\omega$ | relaxation factor in the SOR method |

## REFERENCES


1. J. S. Lee and Y. F. Fung, 'Flow in locally constricted tubes at low Reynolds numbers', *ASME J. Appl. Mech.* **37,** 9–16 (1970).
2. W. L. Oberkampf and S. C. Goh, 'Numerical solution of incompressible viscous flow in irregular tubes', *Proc. Int. Conf. on Computer Methods in Non-linear Mechanics*, University of Texas, Austin, 1974, pp. 569–579.
3. M. D. Desphande, D. P. Giddens and R. F. Mabon, 'Steady laminar flow through modelled vascular stenoses', *J. Biomech.*, **9,** 165–174 (1976).
4. T. J. Mueller, 'Application of numerical methods to physiological flows', in H. J. Wirz and J. J. Smolderen (eds), *Numerical Methods in Fluid Dynamics*, McGraw-Hill, New York, 1978, pp. 89–154.
5. F. T. Smith, 'The separating flow through a severely constricted symmetric tubes', *J. Fluid Mech.*, **90,** 725–754 (1979).
6. S. O. Wille, 'Pressure and flow in arterial stenoses simulated in mathematical models', *Appl. Math. Model.* **4,** 483–488 (1980).
7. I. J. Sobey, 'On flow through furrowed channels. Part 1: Calculated flow patterns', *J. Fluid Mech.* **96,** 1–26 (1980).
8. K. D. Stephanoff, I. J. Sobey and B. J. Bellhouse, 'On flow through furrowed channels, Part 2: Observed flow patterns', *J. Fluid Mech.* **96,** 27–32 (1980).
9. S. A. Ahmed and D. P. Giddens, 'Velocity measurements in steady flow through axisymmetric stenoses at moderate Reynolds number', *J. Biomech.*, **16,** No. 7, 505–516 (1983).
10. M. Siouffi, R. Pelissier, D. Farahifar and R. Rieu, 'The effects of unsteadiness on the flow through stenoses and bifurcations', *J. Biomech.* **17,** 299–315 (1984).
11. A. T. Prata and E. M. Sparrow, 'Heat transfer and fluid flow characteristics for an annulus of periodically varying cross section', *Numer. Heat Transfer*, **7,** 285–304 (1984).
12. S. Tsangaris and E. Leiter, 'On laminar steady flow in sinusoidal channels', *J. Eng. Math.* **18,** 89–103 (1984).
13. V. O'Brien and L. W. Ehrlich, 'Simple pulsatile flow in an artery with a constriction', *J. Biomech.* **18,** 117–127 (1985).
14. L. H. Back, J. R. Radbill and Y. I. Cho, 'Measurement and prediction of flow through a replica segment of a mildly atherosclerotic coronary artery of man', *J. Biomech.* **19,** 1–17 (1986).
15. A. A Samarskii and V. B. Andreev, 'On high accuracy difference scheme for an elliptic equation with several space variables', *USSR Comput. Math. Phys.* **3,** 1373–1382 (1963).
16. J. C. Bentz and N. A. Evans, 'Hemodynamic flow in the region of a simulated stenosis', *ASME Winter Annual Meeting*, Houston, 30 November–4 December 1975, ASME Paper No. 75-WA/BA10-10.